Journal of Catalysis 256 (2008) 301–311

Contents lists available at ScienceDirect

Journal of Catalysis

www.elsevier.com/locate/jcat

Heptacoordinate tricarbonyl Mo(II) complexes as highly selective oxidation homogeneous and heterogeneous catalysts

Maria Vasconcellos-Dias [a], Carla D. Nunes [a,*], Pedro D. Vaz [a], Paula Ferreira [b], Paula Brandão [c], Vítor Félix [c], Maria José Calhorda [a]

[a] Departamento de Química e Bioquímica, CQB, Faculdade de Ciências da Universidade de Lisboa, 1749-016 Lisboa, Portugal
[b] Departamento de Engenharia Cerâmica e do Vidro, CICECO, Universidade de Aveiro, Campus de Santiago, 3810-193 Aveiro, Portugal
[c] Departamento Química, CICECO, Universidade de Aveiro, 3810-193 Aveiro, Portugal

ARTICLE INFO

Article history:
Received 22 November 2007
Revised 25 March 2008
Accepted 25 March 2008
Available online 1 May 2008

Dedicated to Prof. W. Herrmann on the occasion of his 60th birthday

Keywords:
Molybdenum
Mesoporous materials
Selective epoxidation
Catalysis
Oxidation
Polymerization

ABSTRACT

$[MoX_2(CO)_3(pyca)]$ (X = I, Br) complexes bearing the ligand $C_5H_4NCH{=}N(CH_2)_2CH_3$ (pyca, **2**) were prepared and characterized by elemental analysis as well as FTIR and ^1H and ^{13}C solution NMR spectroscopy. Using the modified ligand $C_5H_4NCH{=}N(CH_2)_3Si(OEt)_3$ (pycaSi, **3**), they were immobilized in MCM-41 (**MCM**) and in mesoporous materials (i.e., periodic mesoporous organosilica [PMO]) and then characterized by powder X-ray diffraction, N_2 adsorption analysis, FTIR, and ^{29}Si MAS and CP MAS and ^{13}C CP MAS solid-state NMR spectroscopy. These new materials and complexes were tested in the oxidation of cyclohexene, cyclooctene, and styrene and in the polymerization of styrene and norbornene. All were good catalyst precursors for olefin epoxidation with TBHP (*t*-butylhydroperoxide), leading selectively to epoxides with high conversions and TOFs and achieving high conversions in the second run. This finding, combined with the fact that the materials outperformed the homogeneous complexes, make these catalysts very attractive. They combine the selectivity and activity of the homogeneous species with the features of materials. The iodine-containing materials performed better for styrene (100% conversion), and the bromine-containing materials displayed higher conversion for cyclooctene.

© 2008 Elsevier Inc. All rights reserved.

1. Introduction

Heterogeneous catalysis offers as a main advantage the easy recovery of the catalyst and reaction products, making it the preferred technique in most industrial applications. On the other hand, the selectivity is usually lower than that of many homogeneous systems. The design of more active and more selective heterogeneous catalysts remains a priority. The availability of a large surface is a requirement that can be provided by different kinds of materials, among which mesoporous materials (namely, the MCM family) meet many of the relevant criteria [1,2]. The micelle templated MCM-41 (**MCM**), in particular, is a readily functionalizable silicon-based material with hexagonally ordered parallel channels, a large surface area, and good mechanical stability. Several applications of these materials containing immobilized inorganic complexes have been described, ranging from catalytic studies to photochemistry and electrochemistry studies [3–6].

The nature of the surface walls, determined by the presence of OH groups, allows reaction with many molecules of interest. To obtain a supported catalyst, usually derived from a transition metal derivative, one of two methods can be used: the reaction of a complex containing a suitable ligand (grafting) or the step-by-step approach (tethering), starting with reaction of a ligand with the reactive surface silanols of the wall, followed by interaction with the transition metal precursor. Both methods have been widely tested with good results [7,8].

More recently, the introduction of organic molecules within the inorganic framework has been made possible by a one-step synthetic procedure leading to hybrid organic–inorganic materials known as periodic mesoporous organosilicas (PMO) [9–17]. Silylated precursors containing phenyl rings, thiophene, imidazole, ferrocene molecules, and many other organic groups have been used to form the walls in such a way as to maintain the mesoporous structure [18–27]. Whereas in principle these two synthetic routes should yield the same material, the formation of an ordered structure is highly dependent on the nature and amount of the organic group of the precursor [16,17]. The features of the final materials when comparable quantities of the organic moiety are introduced appear similar in structural terms, but the local order can change; for instance, the hydrophilicity (defining the number of OH groups on the walls) is significantly affected and may influence later reactions, including the catalytic activity of future materials [28].

In previous work, we described the immobilization of the 1,4-diazabutadiene (DAB) ligand RN=C(Ph)–C(Ph)=NR, R=$(CH_2)_3$

* Corresponding author. Fax: +351 217500088.
E-mail address: cmnunes@fc.ul.pt (C.D. Nunes).

0021-9517/$ – see front matter © 2008 Elsevier Inc. All rights reserved.
doi:10.1016/j.jcat.2008.03.023

$Si(OEt)_3$ or $(CH_2)_2CH_3$, and some of its Mn(II) and V(IV) derivatives in **MCM**, using grafting and tethering procedures. Grafting a transition metal complex has proven to be inefficient due to the size of the complex, leading to small metal loads in the final material [7]. On the other hand, the ligand is disilylated and can bind to the walls by one or two arms. Experimental evidence is not totally conclusive, and a final solution to the problem remains elusive. In this work, we used a less symmetric ligand, $C_5H_4NCH{=}NR$, $R{=}(CH_2)_3Si(OEt)_3$, or $(CH_2)_2CH_3$, which can react unambiguously with the wall. It is introduced in **MCM** or used to produce a new hybrid organic–inorganic material (**PMO**) in a one-pot synthesis. These materials functionalized with the diimine ligand react with organometallic complexes $[MoX_2(CO)_3(NCMe)_2]$ (X = Br, I), which have shown catalytic activity in, for instance, olefin polymerization and ring-opening metathesis polymerization, to afford new heterogeneous catalysts [8]. As we show herein, the catalytic activity of the **PMO** materials as precursors in the epoxidation of olefins using as oxidant *t*-butylhydroperoxide (TBHP) exceeds that of both the classical **MCM** grafted materials and, more interestingly, the analogous homogeneous-phase catalyst.

2. Experimental

2.1. General

All reagents were obtained from Aldrich and used as received. Commercial-grade solvents were dried and deoxygenated by standard procedures (i.e., Et_2O, THF, and toluene over Na/benzophenone ketyl; CH_2Cl_2 over CaH_2), distilled under nitrogen, and kept over 4 Å molecular sieves. The organometallic complexes $[MoX_2(CO)_3(NCCH_3)_2]$ (X = I, **1a**, X = Br, **1b**) were prepared as reported [29]. Ligands $C_5H_4NCH{=}N(CH_2)_2CH_3$ (pyca, **2**) and $C_5H_4NCH{=}N(CH_2)_3Si(OEt)_3$ (pycaSi, **3**) were prepared as described below. MCM-41 and postsynthetic derivatized materials were synthesized as described previously, using $[(C_{16}H_{33})N(CH_3)_3]Br$ (CTAB) as the templating agent [30]. Before the grafting experiment, physisorbed water was removed from calcined (813 K for 6 h under air) **MCM** by heating at 453 K in vacuum (10^{-2} Pa) for 2 h. Hybrid materials also were prepared using ligand **3** as described previously with an organic material load of 2.7% [16,17]. FTIR spectra were obtained as KBr pellets and diffuse reflectance measurements (DRIFT) using 1 cm^{-1} resolution on a Nicolet 6700 in the 400–4000 cm^{-1} range. Powder XRD measurements were taken on a Philips PW1710 using Cu$K\alpha$ radiation filtered by graphite. ^1H and ^{13}C solution NMR spectra were obtained with a Bruker Avance 400 spectrometer. ^{29}Si and ^{13}C solid-state NMR spectra were recorded at 79.49 MHz and 100.62 MHz, respectively, on a (9.4 T) Bruker Avance 400P spectrometer. ^{29}Si MAS NMR spectra were recorded with 40° pulses, spinning rates of 5.0–5.5 kHz, and 60 s recycle delays. ^{29}Si CP MAS NMR spectra were recorded with 5.5 μs ^1H 90° pulses, 8 ms contact time, a spinning rate of 4.5 kHz, and 4 s recycle delays. ^{13}C CP MAS NMR spectra were recorded with a 4.5 μs ^1H 90° pulse, 2 ms contact time, a spinning rate of 8 kHz, and 4 s recycle delays. Chemical shifts are quoted in ppm from TMS. ^{13}C spectra were also recorded in the solid-state at 125.76 MHz on a Bruker Avance 500 spectrometer. The N_2 sorption measurements were obtained in an automatic apparatus (ASAP 2010; Micromeritics). BET specific surface areas (S_{BET}, $p/p0$ from 0.03 to 0.13) and specific total pore volume, Vp, were estimated from N_2 adsorption isotherms measured at 77 K. The pore size distributions (PSD) were calculated by the BJH method using the modified Kelvin equation, with correction for the statistical film thickness on the pore walls [31,32]. The statistical film thickness was calculated using the Harkins–Jura equation in the $p/p0$ range from 0.1 to 0.95. Microanalyses were performed at the University of Vigo and University of Aveiro.

2.2. Catalytic studies

The complexes and materials reported herein were tested in the ROMP of norbornene (NBE) and polymerization of styrene (Sty) under N_2 atmosphere at 333 K and using toluene as solvent. The polymers were precipitated by addition of methanol at the end of the reaction (i.e., after 48 h and catalyst separation). The catalytic reactions using complexes $[MoI_2(CO)_3(pyca)]$ (**4a**) and $[MoBr_2(CO)_3(pyca)]$ (**4b**) were carried out using a catalyst/olefin molar ratio of 1:200. In the studies using the composite materials **6** (**a, b**) and **8** (**a, b**) a Mo/olefin molar ratio of 1:200 (based on the metal loadings as determined by ICP-AES) was used. For the catalytic reaction using MAO as a co-catalyst, the Mo/Al/olefin molar ratio was 1:3:200. In a typical experiment, a specific amount of the material with 18.5 mmol of olefin was mixed in toluene (10 mL) at 333 K. All of the reactions were stopped after 48 h. This was accomplished by separating the catalysts by filtration, followed by the addition of methanol to the toluene solution to precipitate the polymer. The solid polymer was separated by filtration, and the polymers were dried in vacuum before being weighed. The yields were calculated based on the initial weight of olefin used. The polymers were identified by ^1H NMR, and the *cis* content (NBE) and tacticity (Sty) was estimated from ^1H and ^{13}C NMR data [33–37].

The complexes and materials also were tested in the epoxidation of olefins (*cis*-cyclooctene, cyclohexene, and styrene), using as oxidant *t*-butylhydroperoxide (TBHP). The catalytic oxidation of the different olefins was carried out at 328 K under normal atmosphere in a reaction vessel equipped with a magnetic stirrer and a condenser. Some control experiments were conducted under inert N_2 atmosphere to evaluate whether molecular O_2 from air would interfere. The vessel was loaded with olefin (100%), internal standard (DBE), catalyst (1%), oxidant (200%), and 3 mL of solvent. The addition of the oxidant determines the initial time of the reaction. The course of the reaction was monitored by quantitative gas chromatography (GC) analysis. Samples were obtained every 15 min during the first hour and then after 2, 4, 6, 8, and 24 h of reaction. The samples were diluted with dichloromethane and chilled in an ice bath.

For the destruction of *t*-butylhydroperoxide, a catalytic amount of manganese dioxide was added. The resulting slurry was filtered, and the filtrate was injected into the gas chromatograph column. The conversion of each olefin (measured by the formation of the corresponding epoxide) was quantified by GC from calibration curves recorded before the reaction. The presence of other reaction byproducts also was determined by NMR spectroscopy and GC–MS by comparing the catalytic mixture with standard samples. Blank experiments using TBHP/MnO_2 and olefin were carried out; no measurable activity was found. No reaction occurred without a metal-containing catalyst. The catalyst reusability was evaluated by running a second reaction cycle after 24 h without catalyst separation and then recharging equimolar amounts of cyclooctene and TBHP. The course of the reaction was monitored as before.

2.2.1. Epoxidation of cis-cyclooctene

cis-Cyclooctene (800 mg, 7.3 mmol), 800 mg dibutyl ether (internal standard), 1 mol% of catalyst, 2.65 mL of TBHP (5.5 M in *n*-decane), and 3 mL of CH_2Cl_2.

2.2.2. Epoxidation of cyclohexene

Cyclohexene (800 mg, 9.7 mmol), 800 mg dibutyl ether (internal standard), 1 mol% of catalyst, 2.65 mL of TBHP (5.5 M in *n*-decane), and 3 mL of CH_2Cl_2.

2.2.3. Epoxidation of styrene

Styrene (800 mg, 7.7 mmol), 800 mg dibutyl ether (internal standard), 1 mol% of catalyst, 2.65 mL of TBHP (5.5 M in *n*-decane), and 3 mL of CH_2Cl_2.

*2.3. Preparation of $C_5H_4NCH{=}N(CH_2)_2CH_3$ (pyca, **2**)*

A solution of propylamine (0.986 mL, 12 mmol) in dry THF (10 mL) was added to a solution of pyridine-2-carbaldehyde (0.951 mL, 10 mmol) in dry THF, followed by 4 Å molecular sieves (1.6 mm pellets, 0.6 g), and a catalytic amount of $ZnCl_2$. After 12 h at 323 K, the solution was filtered, the resultant residue was rinsed with THF, and the filtrate was evaporated in vacuum to give the product, which was recrystallized from chloroform as a white solid (1.25 g) in 85% yield. Elemental analysis (%) $C_9H_{12}N_2$ (148.0): calcd. C 72.94, N 18.90, H 8.44; found C 72.66, N 18.74, H 8.06. IR (KBr ν cm^{-1}): 3069 (m), 3022 (m), 2966 (s), 2932 (s), 2873 (s), 1647 (vs), 1596 (vs), 1570 (m), 1479 (s), 1447 (s), 1357 (w), 1304 (vs), 1270 (m), 1225 (s), 1159 (m), 1110 (s), 1048 (s), 1016 (vs), 989 (s), 907 (w), 891 (w), 862 (w), 784 (vs), 748 (m), 679 (w), 640 (m), 549 (w), 500 (s). ^{1}H NMR (400.13 MHz, $CDCl_3$, 298 K, δ ppm TMS): 0.98 (t, 3H, H_{10}), 1.87 (t, 2H, H_9), 3.79 (t, 2H, H_8), 7.66 (s, 1H, H_7), 7.97 (d, 1H, H_5), 8.06 (d, 1H, H_3), 8.50 (s, 1H, H_4), 8.79 (d, 1H, H_6). $^{13}C\{^1H\}$ NMR (100.61 MHz, $CDCl_3$, 298 K, δ ppm TMS): 11.6 (C_{10}), 23.4 (C_9), 61.4 (C_8), 125.3 (C_3), 127.6 (C_5), 139.8 (C_4), 148.0 (C_6), 149.7 (C_2), 160.9 (C_7).

*2.4. Preparation of $C_5H_4NCH{=}N(CH_2)_3Si(OEt)_3$ (pycaSi, **3**)*

A solution of (3-aminopropyl)triethoxysilane (1.42 g, 6.4 mmol) in dry THF (10 mL) was added to a solution of pyridine-2-carbaldehyde (0.61 mL, 6.4 mmol) in dry THF, followed by 4 Å molecular sieves (1.6 mm pellets, 0.6 g), and a catalytic amount of $ZnCl_2$. After 12 h at 323 K, the solution was filtered, the resultant residue was rinsed with THF, and the filtrate was evaporated in vacuum to give a pale-yellow oil as the product (1.68 g) in 89% yield. Elemental analysis (%) $C_{15}H_{26}N_2O_3Si$ (296.0): calcd. C 58.02, N 9.02, H 8.44; found C 58.35, N 9.19, H 8.48. IR (KBr ν cm^{-1}): 2975 (s), 2927 (s), 2885 (s), 1651 (s), 1626 (s), 1598 (vs), 1570 (m), 1481 (m), 1457 (m), 1442 (s), 1390 (vs), 1368 (w), 1348 (w), 1304 (m), 1281 (m), 1191 (vs), 1167 (vs), 1102 (vs), 1079 (vs), 1027 (w), 1018 (w), 988 (w), 958 (vs), 894 (m), 882 (m), 857 (m), 781 (vs), 681 (w), 660 (m), 639 (s), 546 (m), 501 (w), 475 (w). ^{1}H NMR (400.13 MHz, $CDCl_3$, 298 K, δ ppm TMS): 0.69 (t, 2H, H_{10}), 1.22 (t, 9H, OCH_2CH_3), 1.63–1.82 (m, 2H, H_9), 1.98 (t, 2H, H_8), 3.81–3.87 (m, 6H, OCH_2CH_3), 7.57 (s, 1H, H_7), 7.91 (t, 2H, H_5, H_3), 8.42 (s, 1H, H_4), 8.74 (s, 1H, H_6). $^{13}C\{^1H\}$ NMR (100.61 MHz, $CDCl_3$, 298 K, δ ppm TMS): 7.9 (C_{10}), 18.3 (OCH_2CH_3), 24.1 (C_9), 58.4 (C_8), 64.1 (OCH_2CH_3), 121.3 (C_3), 124.7 (C_5), 136.6 (C_4), 148.0 (C_6), 149.7 (C_2), 161.9 (C_7).

*2.5. Preparation of the complexes $[MoX_2(CO)_3(pyca)]$, X = I (**4a**), Br (**4b**)*

A solution of $[MoI_2(CO)_3(NCCH_3)_2]$ (**1a**) or $[MoBr_2(CO)_3(NCCH_3)_2]$ (**1b**) (1.00 mmol) in MeOH (10 mL) was treated with a solution of the ligand pyca **2** (1.05 mmol; 160 mg) in MeOH (5 mL). The resulting solution was stirred for 14 h at room temperature and evaporated to dryness. A brown solid was obtained, washed with hexane, and dried under vacuum.

4a Yield: (0.272g) 92%. Elemental analysis (%) $C_{12}H_{12}N_2O_3I_2Mo$ (581.98): calcd. C 24.77, H 2.08, N 4.81; found C 24.57, H 1.99, N 4.61. IR (KBr, ν cm^{-1}): 2965 (w), 2874 (w), 2033 (s), 2014 (s), 1967 (s), 1899 (m), 1825 (m), 1613 (vs), 1466 (m), 1445 (m), 1380 (w), 1302 (m), 1232 (m), 1158 (m), 1109 (w), 968 (m), 767 (s), 747 (m), 516 (w). ^{1}H NMR (400.10 MHz, $CDCl_3$, r.t., δ ppm TMS): 0.92 (t, 3H, H_{10}), 1.59 (m, 2H, H_9), 2.80 (t, 2H, H_8), 5.88 (s, 1H, H_7), 8.12 (m, 2H, H_3, H_5), 8.69 (m, 2H, H_6, H_4). $^{13}C\{^1H\}$ NMR (100.61 MHz, $CDCl_3$, 298 K, δ ppm TMS): 11.2 (C_{10}), 22.0 (C_9), 42.4 (C_8), 93.7 (C_7), 126.8 (C_3), 128.3 (C_5), 141.4 (C_4), 142.2 (C_6), 148.7 (C_2).

4b Yield: (0.217g) 88%. Elemental analysis (%) $C_{12}H_{12}N_2O_3Br_2Mo$ (487.98): calcd. C 29.53, H 2.48, N 5.74; found C 29.97, H 1.89, N 5.61. IR (KBr, ν cm^{-1}): 2964 (w), 2874 (w), 2033 (s), 2011 (s), 1971 (s), 1899 (m), 1829 (m), 1617 (vs), 1473 (m), 1458 (m), 1379 (w), 1302 (m), 1261 (m), 1231 (m), 1158 (m), 1106 (w), 1022 (m), 968 (m), 770 (s), 507 (w). ^{1}H NMR (400.10 MHz, $CDCl_3$, r.t., δ ppm TMS): 0.90 (t, 3H, H_{10}), 1.51–1.61 (m, 2H, H_9), 2.77 (t, 2H, H_8), 5.73 (d, 1H, H_7), 7.88–7.95 (m, 1H, H_5), 8.03 (d, 1H, H_3), 8.43–8.55 (m, 1H, H_6), 8.63 (d, 1H, H_4). $^{13}C\{^1H\}$ NMR (100.61 MHz, $CDCl_3$, 298 K, δ ppm TMS): 11.1 (C_{10}), 21.8 (C_9), 42.5 (C_8), 94.2 (C_7), 127.9 (C_3), 129.3 (C_5), 143.7 (C_4), 144.7 (C_6), 153.7 (C_2).

*2.6. Preparation of MCM–pycaSi (**5**)*

A solution of **3** (0.70 g, 1.13 mmol) in toluene (10 mL) was added to a suspension of MCM-41 (0.8 g) in toluene (10 mL), and the mixture was heated at 373 K for 9 h. The resulting solid was filtered off and washed four times with CH_2Cl_2 (4 × 15 mL), then dried in vacuum at 323 K for 3 h. Elemental analysis (%): found C 9.97, N 1.60, H 1.82. IR (KBr, ν cm^{-1}): 3400 (vs), 2980 (w), 2936 (vw), 2900 (vw), 1717 (vw), 1652 (w), 1603 (w), 1573 (w), 1475 (w), 1448 (w), 1394 (w), 1243 (s), 1084 (vs), 967 (m), 810 (s), 575 (m), 463 (s). ^{13}C CP MAS NMR (δ ppm): 9.5 ($SiCH_2$), 16.1 ($SiCH_2CH_3$), 21.2 ($CH_2CH_2CH_3$), 42.8 (CH_2N), 57.8 (OCH_2CH_3), 127.7, 140.6, 147.2, 149.4 (Ph-C), 162.3 (HC=N). ^{29}Si MAS NMR (δ ppm): −58.8 (T^1), −94.5 (Q^2), −102.7 (Q^3), −109.6 (Q^4). ^{29}Si CP MAS NMR (δ ppm): −58.1 (T^1), −60.6 (T^2), −66.7 (T^3), −92.9 (Q^2), −102.7 (Q^3), −110.3 (Q^4).

*2.7. Preparation of MCM–pycaSi–MoX_2, X = I (**6a**), Br (**6b**)*

A solution of $[MoI_2(CO)_3(NCCH_3)_2]$ (**1a**) or $[MoBr_2(CO)_3(NCCH_3)_2]$ (**1b**) (0.65 mmol) in dry CH_2Cl_2 (5 mL) was added to a suspension of 1.00 g of the material **MCM–pycaSi** (**5**) in dry CH_2Cl_2 (20 mL). The reaction mixture was stirred under a N_2 atmosphere at room temperature overnight. The resulting material was then filtered off, washed twice with CH_2Cl_2 (2 × 20 mL), and dried under vacuum.

6a Elemental analysis (%): found C 7.17, N 1.41, H 1.59, Mo 3.02. IR (KBr, ν cm^{-1}): 3460 (vs), 2980 (w), 2960 (w), 2930 (w), 1990 (s), 1880 (s), 1640 (vs), 1530 (m), 1470 (s), 1383 (s), 1400 (m), 1240 (vs), 1090 (vs), 972 (m), 812 (m), 460 (s). ^{13}C CP MAS NMR (δ ppm): 9.5 ($SiCH_2$), 16.5 ($SiOCH_2CH_3$), 21.2 ($CH_2CH_2CH_2$), 42.9 (CH_2N), 58.4 ($SiOCH_2CH_3$), 126.5, 142.7, 147.6 (Ph). ^{29}Si MAS NMR (δ ppm): −54.7 (T^1), −57.4 (T^2), −62.1 (T^3), −97.6 (Q^2), −104.3 (Q^3), −110.5 (Q^4). ^{29}Si CP MAS NMR (δ ppm): −53.6 (T^1), −58.4 (T^2), −63.2 (T^3), −92.0 (Q^2), −102.7 (Q^3), −108.7 (Q^4).

6b Elemental analysis (%): found C 7.77, N 1.67, H 1.56, Mo 5.4. IR (KBr, ν cm^{-1}): 2970 (w), 2940 (w), 2010 (m), 1980 (s), 1910 (s), 1840 (s), 1620 (vs), 1570 (m), 1480 (w), 1470 (m), 1460 (m), 1380 (s), 1300 (m), 1260 (m), 1230 (m), 1160 (m), 1110 (m), 1060 (m), 1030 (m), 972 (s), 870 (m), 770 (vs), 594 (m). ^{13}C CP MAS NMR (δ ppm): 9.8 ($SiCH_2$), 17.9 ($SiOCH_2CH_3$), 20.8 ($CH_2CH_2CH_2$), 42.7 (CH_2N), 58.1 ($SiOCH_2CH_3$), 126.2, 141.0 (Ph). ^{29}Si MAS NMR (δ ppm): −54.7 (T^1), −57.8 (T^2), −64.4 (T^3), −94.4 (Q^2), −102.6 (Q^3), −110.1 (Q^4). ^{29}Si CP MAS NMR (δ ppm): −51.9 (T^1), −58.6 (T^2), −63.1 (T^3), −95.2 (Q^2), −103.4 (Q^3), −109.9 (Q^4).

2.8. Preparation of PMO–pycaSi (**7**)

An aqueous solution of ethylamine was added to a stirred solution of CTAB. Then a mixture of tetraethylorthosilicate (TEOS) and **3** in MeOH was added dropwise, leading to a composition in molar ratio of 1:0.027:0.14:2.4:2:100 SiO_2/**3**/CTAB/$EtNH_2$/MeOH/H_2O. The reaction mixture was stirred for another 4 h at room temperature, then heated to 373 K for 24 h. The product was recovered by filtration, washed thoroughly with distilled water, and dried under ambient conditions. The surfactant was extracted by stirring twice (to ensure maximum extraction) 3.0 g of the synthesized hybrid material in 250 mL of MeOH and 6.0 g of an aqueous solution of HCl (37%) at 323 K for 6 h. The resulting solid was then filtered, washed with MeOH, and dried in air at 373 K. Elemental analysis (%): found C 3.36, N 0.41, H 1.27. IR (KBr, ν cm^{-1}): 3440 (vs), 2978 (vw), 2959 (vw), 1971 (vw), 1886 (vw), 1652 (w), 1630 (m), 1571 (vw), 1472 (vw), 1387 (vw), 1230 (s), 1082 (vs), 945 (s), 805 (s), 557 (m), 457 (s). ^{13}C CP MAS NMR (δ ppm): 8.8 ($SiCH_2$), 16.4 ($SiOCH_2CH_3$), 21.1 ($CH_2CH_2CH_2$), 42.4 (CH_2N), 49.0 ($SiOCH_2CH_3$). ^{29}Si MAS NMR (δ ppm): −92.4 (Q^2), −100.6 (Q^3), −109.9 (Q^4). ^{29}Si CP MAS NMR (δ ppm): −66.0 (T), −91.1 (Q^2), −100.6 (Q^3), −110.1 (Q^4).

2.9. Preparation of PMO–pycaSi–MoX_2, X = I (***8a***), Br (***8b***)

A solution of $[MoI_2(CO)_3(NCCH_3)_2]$ (**1a**) or $[MoBr_2(CO)_3(NCCH_3)_2]$ (**1b**) (0.65 mmol) in dry CH_2Cl_2 (5 mL) was added to a suspension of 1.00 g of the material **PMO–pycaSi** (**7**) in dry CH_2Cl_2 (20 mL). The reaction mixture was stirred under a N_2 atmosphere at room temperature overnight. The resulting material was then filtered off, washed twice with CH_2Cl_2 (2 × 20 mL), and dried under vacuum during several hours.

8a Elemental analysis (%): found C 3.92, N 0.46, H 1.56, Mo 2.72. IR (KBr, ν cm^{-1}): 3480 (vs), 2990 (w), 2920 (w), 2870 (w), 2000 (m), 1880 (m), 1710 (m), 1640 (s), 1630 (s), 1520 (m), 1470 (m), 1410 (s), 1220 (s), 1090 (s), 973 (m), 808 (m), 463 (s). ^{13}C CP MAS NMR (δ ppm): 9.1 ($SiCH_2$), 15.9 ($SiOCH_2CH_3$), 21.0 ($CH_2CH_2CH_2$), 42.7 (CH_2N), 58.4 ($SiOCH_2CH_3$). ^{29}Si MAS NMR (δ ppm): −92.6 (Q^2), −101.8 (Q^3), −111.8 (Q^4). ^{29}Si CP MAS NMR (δ ppm): −68.8 (T), −94.1 (Q^2), −101.4 (Q^3), −111.2 (Q^4).

8b Elemental analysis (%): found C 2.97, N 0.8, H 2.00, Mo 3.9. IR (KBr, ν cm^{-1}): 2997 (vw), 2976 (vw), 2085 (vw), 1992 (vs), 1929 (s), 1862 (s), 1633 (s), 1516 (w), 1475 (w), 1421 (w), 1240 (vs), 1084 (vs), 968 (vs), 810 (vs), 594 (m). ^{13}C CP MAS NMR (δ ppm): 8.6 ($SiCH_2$), 10.9 ($SiOCH_2CH_3$), 20.5 ($CH_2CH_2CH_2$), 42.2 (CH_2N), 57.8 ($SiOCH_2CH_3$). ^{29}Si MAS NMR (δ ppm): −51.9 (T^1), −57.4 (T^2), −63.6 (T^3), −95.4 (Q^2), −100.7 (Q^3), −110.6 (Q^4). ^{29}Si CP MAS NMR (δ ppm): −53.7 (T^1), −56.6 (T^2), −62.5 (T^3), −95.6 (Q^2), −101.5 (Q^3), −110.4 (Q^4).

2.10. Crystallography

Crystals suitable for single-crystal XRD structure determination were grown from a $CDCl_3$ solution of ligand **2** (pyca) in an NMR tube.

Crystal data: $C_9H_{12}Cl_2N_2Zn$, Mr = 284.48, monoclinic, space group $P2_1/c$ (N° 14), $Z = 4$, $a = 9.3768(3)$ Å, $b = 17.3317(5)$ Å, $c = 7.9682(2)$ Å, $\beta = 113.221(1)°$, $U = 1190.06(6)$ $Å^3$, $T = 100(2)$ K, ρ(calc) = 1.588 $Mg\,m^{-3}$, (Mo$K\alpha$) 2.476 mm^{-1}. 35,319 intensities collected, 3022 independent reflections (R_{int} of 0.0340), which were used in solution and structure refinement. The final R and R_w indices were $R_1 = 0.0216$ and $wR_2 = 0.0546$ for 3022 reflections with $I > 2\sigma(I)$ and $R_1 = 0.0249$ and $wR_2 = 0.0546$ for all *hkl* data.

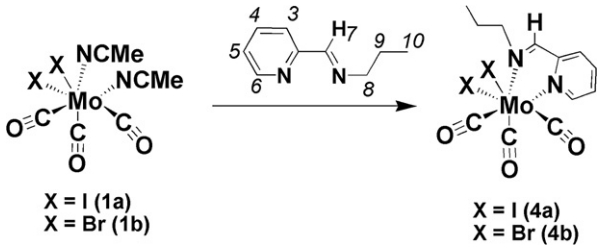

Scheme 1. Formation of complexes $[MoX_2(CO)_3(pyca)]$ (X = I, **4a**, X = Br, **4b**).

The X-ray data were collected at room temperature on a Bruker APEX II CCD using graphite monochromatized Mo$K\alpha$ radiation ($\lambda = 0.71073$ Å) with the crystal positioned at 35 mm from the CCD, and the spots were measured using a counting time of 5 s. Data reduction and empirical absorption were carried out using a Bruker AXS SAINT-NT. The structure was solved by direct methods and by subsequent difference Fourier syntheses and refined by full matrix least squares on F^2 using the SHELX-97 system programs [38]. Anisotropic thermal parameters were used for all nonhydrogen atoms. Hydrogen atoms bonded to the carbon atoms were included in the refinement in calculated positions with isotropic parameters equivalent to 1.2 times those of the atom to which they are attached. The molecular diagrams presented were drawn using the PLATON graphing software [39].

3. Results and discussion

3.1. Chemical studies: Molecules

The organometallic complexes $[MoX_2(CO)_3(NCCH_3)_2]$ (X = I, **1a**, X = Br, **1b**) reacted with ligand **2** according to the reaction in Scheme 1 (with numbering of the ligand **2**). Ligand **2**, $C_5H_4NCH{=}N(CH_2)_2CH_3$ (pyca), was obtained from the reaction between propylamine and pyridine-2-carbaldehyde in THF, catalyzed by $ZnCl_2$ [40]. To prepare the silylated derivative **3** $C_5H_4NCH{=}N(CH_2)_3Si(OEt)_3$ (pycaSi), 3-aminopropyl-triethoxysilane was used in a similar reaction. The formation of **2** was demonstrated by the FTIR spectrum, namely the new ν(C=N) mode of the imine at 1596 cm^{-1}. Bands at 2966, 2932, and 2873 cm^{-1} due to the ν(C–H) modes of the aliphatic chain, as well as bands at 3069 and 3022 cm^{-1} due to ν(C–H) modes of the aromatic moiety, also were observed.

The ^1H NMR spectrum of **2** exhibited peaks at 8.79, 8.50, 8.06, and 7.97 ppm assigned to the protons of the pyridine ring, H_6, H_4, H_3, and H_5, respectively, with the imine proton (H_7) at 7.66 ppm. The protons of the propyl chain appeared at 3.79 (H_8), 1.87 (H_9), and 0.98 (H_{10}) ppm.

The most relevant feature in the ^{13}C NMR spectrum of **2** is a signal at 160.9 ppm assigned to C_7, which was observed at 193 ppm in the aldehyde precursor. The signals of C_6, C_4, C_5, C_3, and C_2 appeared at 148.0, 139.8, 127.6, 125.3, and 149.7 ppm, respectively, and those of the C_8, C_9, and C_{10} groups in the propyl chain appeared at 61.4, 23.5, and 11.6 ppm, respectively.

Some crystals suitable for X-ray single-crystal analysis grew in an NMR tube and were shown to be the complex $[ZnCl_2(pyca)]$. The ^1H and ^{13}C NMR spectra of this complex differed from that described above for free **2**.

Fig. 1 shows the molecular structure of this compound with the labeling scheme adopted in this study. Table 1 gives selected bond distances and angles in the metal coordination sphere. The coordination environment around of Zn^{2+} center, composed of two chlorines and two nitrogen donors from pyca, can be described as a distorted tetrahedron; however, the N–Zn–N angle shows a strong deviation of 28.78(5)° from the ideal value of 109.5° for a

tetrahedron, due to the small bite angle of pyca. The remaining angles subtended at the metal center are within the expected ranges.

The crystal packing diagram of [$ZnCl_2$(pyca)] reveals that pairs of molecules related by the crystallographic inversion center are self-assembled *via* π–π stacking interactions, as shown in Fig. 2. The distance between the two aromatic rings is 3.34 Å.

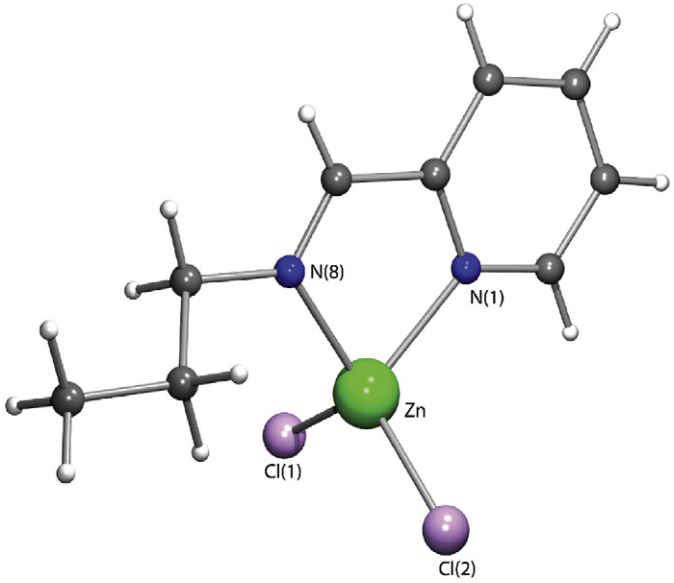

Fig. 1. Molecular structure of the distorted [$ZnCl_2$(pyca)] tetrahedral complex.

Table 1
Selected bond distances (Å) and angles (°) for [$ZnCl_2$(pyca)]

Zn-N(1)	2.070(1)	Zn-N(8)	2.047(1)
Zn-Cl(1)	2.2077(4)	Zn-Cl(2)	2.1983(4)
Cl(2)-Zn-Cl(1)	116.64(2)	N(8)-Zn-N(1)	80.72(5)
N(8)-Zn-Cl(1)	109.97(4)	N(1)-Zn-Cl(1)	113.73(4)
N(8)-Zn-Cl(2)	120.98(4)	N(1)-Zn-Cl(2)	109.51(4)

Ligand **3** was characterized as ligand **2** with similar results (see Section 2). The organometallic complex [$MoI_2(CO)_3$(pyca)] (**4a**) resulted from reaction of complex [$MoI_2(CO)_3(NCCH_3)_2$] (**1a**) with ligand **2**. The most relevant signals in the FTIR spectrum were the three bands assigned to the ν(C≡O) modes at 2033, 2014, and 1967 cm^{-1}, and the ν(C=N) bands of the pyca ligand **2** shifted to 1613 and 1685 cm^{-1}.

In the ^1H NMR, the imine proton H_7 signal shifted from 7.66 ppm in the free ligand **2** to 5.88 ppm in **4a**, whereas the signal of the corresponding carbon atom in the ^{13}C NMR shifted from 160.9 ppm to 93.7 ppm. The peaks of the pyridine ring protons also shifted, to 8.12 (H_3, H_5) and 8.69 (H_4, H_6).

The spectroscopic characterization of complex [$MoBr_2(CO)_3$-(pyca)] (**4b**) by ^1H, ^{13}C NMR and FTIR led to similar results (see Section 2).

3.2. Chemical studies: Materials

Two routes were pursued in the synthesis of the materials, as depicted in Scheme 2. In the first route, pure siliceous MCM-41 (**MCM**) was obtained by a template approach [30], and

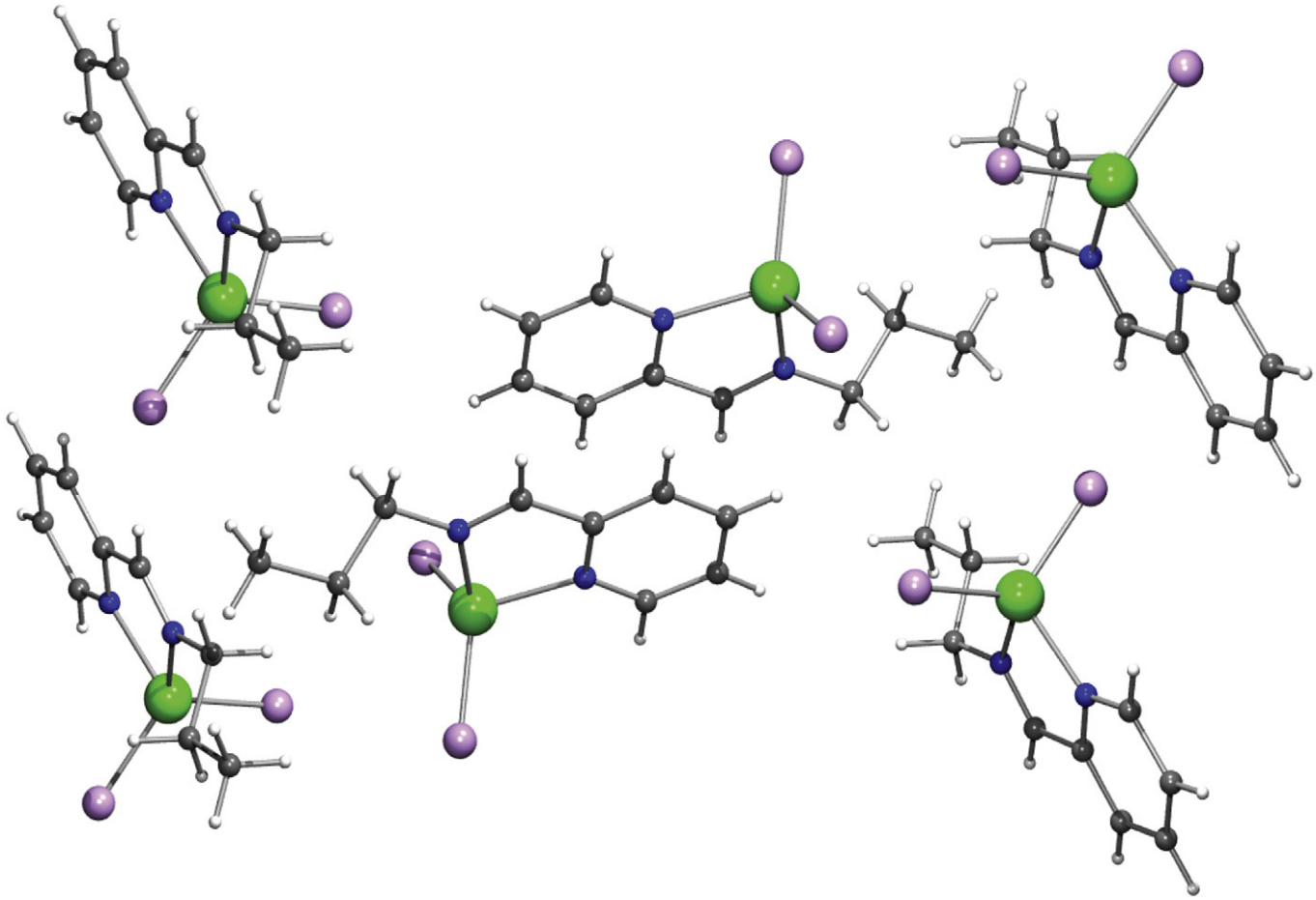

Fig. 2. Unit cell view of [$ZnCl_2$(pyca)] showing the formation of a dimer of [$ZnCl_2$(pyca)], stabilized by π–π stacking interactions.

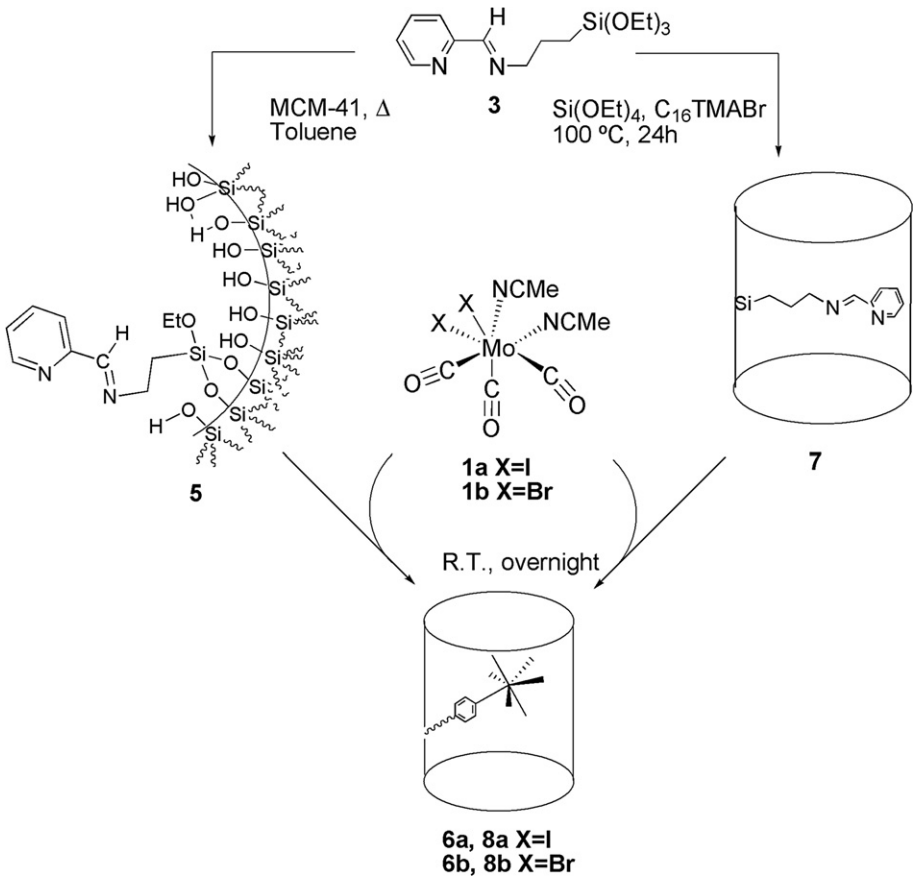

Scheme 2. The two alternative routes to immobilize $[MoX_2(CO)_3]$ (X = I, **4a**, X = Br, **4b**), forming MCM–pycaSi–MoX_2 (X = I, **6a**, X = Br, **6b**) and PMO–pycaSi–MoX_2 (X = I, **8a**, X = Br, **8b**).

then the silica-matrix mesoporous host material was derivatized with ligand **3**, yielding **MCM–pycaSi**, **5** [40]. Treatment of **MCM–pycaSi** (**5**) with a solution of the organometallic complexes $[MoX_2(CO)_3(NCCH_3)_2]$ (X = I, **1a** or X = Br, **1b**) in dichloromethane led to the new materials **MCM–pycaSi–MoX$_2$** (X = I, **6a**, X = Br, **6b**), containing approximately 3.02 wt% Mo (0.31 mmol g^{-1}) for material **6a** and 5.4 wt% Mo (0.55 mmol g^{-1}) for material **6b**.

In the second route, the material is synthesized by co-condensation of the organic ligand **3** with the silica source (TEOS) in a one-pot synthetic procedure. The resulting hybrid material is a modified periodic mesoporous silica, **PMO–pycaSi** (**7**). This synthetic route has been described by Jia et al. [25], with $EtNH_2$ replacing NaOH to avoid contamination with Na^+ ions in the final mesoporous material. Methanol was used as a solvent for TEOS and the ligand, a procedure that seems to prevent phase separation and promote ordering of the material [16,41], and excess template was removed with MeOH/aqueous HCl. The organic building block/TEOS molar ratio chosen for the preparation of the PMO material was of 0.027, which has been shown to produce a well-ordered material with a reasonable content in organic molecule (pyca in this case) [16,25]. Treatment of **PMO–pycaSi** (**7**) with a solution of $[MoX_2(CO)_3(NCCH_3)_2]$ (X = I, **1a**, X = Br, **1b**) in dichloromethane led to the new materials **PMO–pycaSi–MoX$_2$** (X = I, **8a**, X = Br, **8b**), with approximately 2.72 wt% Mo for material **8a** (0.28 mmol g^{-1}) and 3.90 (0.40 mmol g^{-1}) for material **8b**.

The composite materials containing $MoBr_2(CO)_3$, **6b** and **8b**, exhibited spectroscopic features similar to those of the analogues with $MoI_2(CO)_3$ (materials **6a** and **8a**). Consequently, we provide a detailed discussion only of the latter (see Section 2).

The FTIR spectrum (Fig. 3) of the grafted material **MCM–pycaSi** (**5**) shows the stretching vibration modes of the mesoporous framework (Si–O–Si) at around 1243, 1084, and 810 cm^{-1};

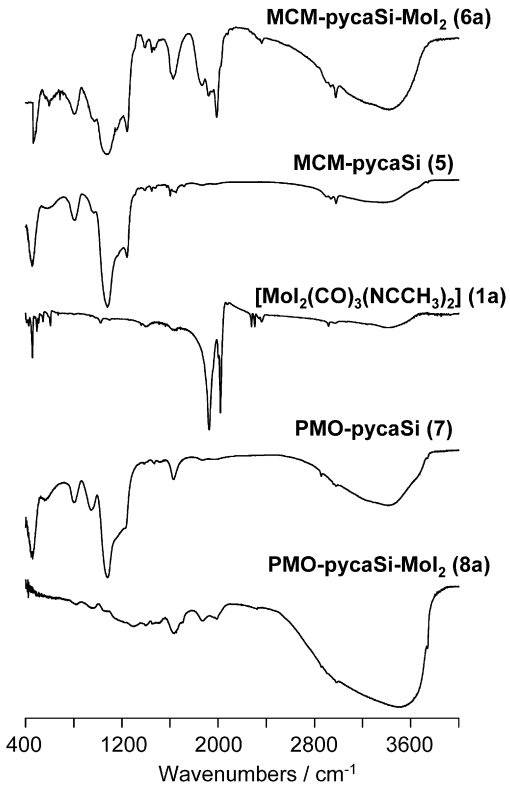

Fig. 3. FTIR spectra of the complex **1a** and all materials containing the MoI_2 fragment.

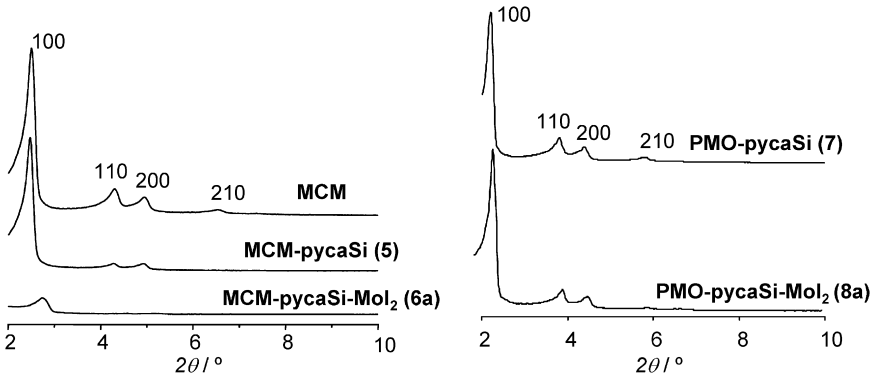

Fig. 4. Powder XRD of the materials: **MCM**, **MCM–pycaSi** (**5**), and **MCM–pycaSi–MoI$_2$** (**6a**) (left); **PMO–pycaSi** (**7**), and **PMO–pycaSi–MoI$_2$** (**8a**) (right).

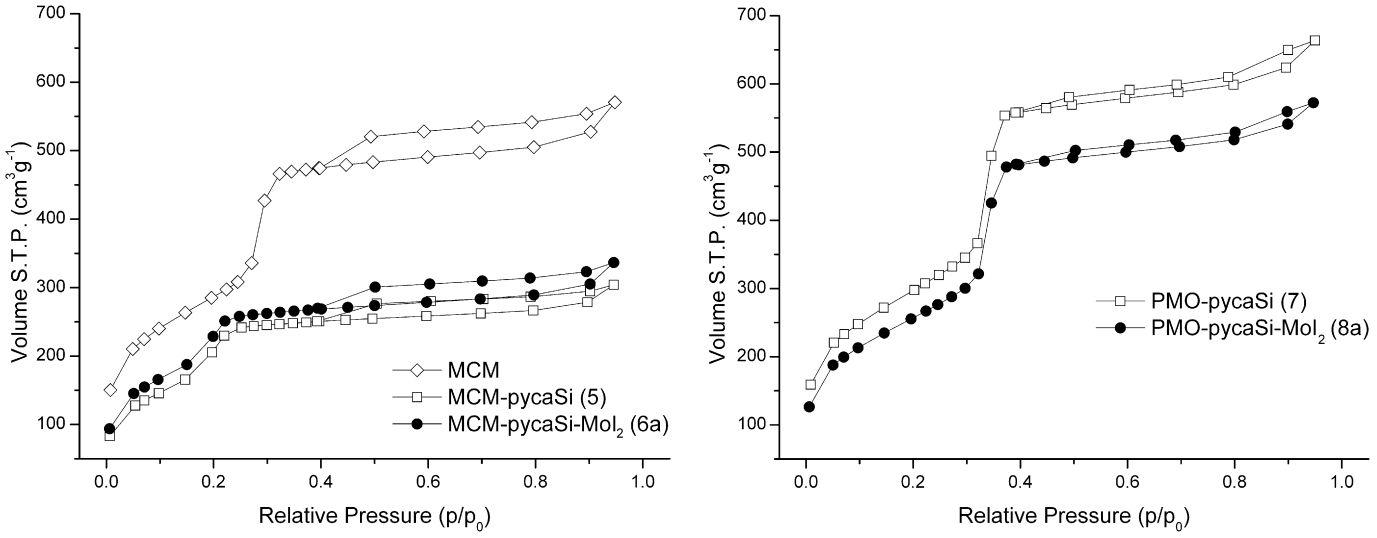

Fig. 5. Nitrogen adsorption studies of the materials at 77 K.

bands at 1652 and 1603 cm^{-1} that can be assigned to the ν(C=N) stretching of the ligand **pycaSi** (**3**); and bands at 2980, 2936, and 2900 cm^{-1} assigned to ν(C–H) stretching of the aliphatic carbons of the linear chain. After binding of the organometallic fragment, it is possible to assign bands at 1240, 1090, and 812 cm^{-1} in **MCM–pycaSi–MoI$_2$** (**6a**) to the asymmetric vibration mode of Si–O–Si and the ν(C=N) stretching modes of the pyca ligand at 1530 and 1640 cm^{-1}, shifted from their values in **MCM–pycaSi** (**5**). The ν(C≡O) modes of the organometallic fragment appeared at around 1990 cm^{-1}.

In the PMO materials, the very strong stretching vibrations of the Si–O–Si framework were observed at 1230, 1082, and 805 cm^{-1} in **PMO–pycaSi** (**7**) and at 1220, 1090, and 808 cm^{-1} in **PMO–pycaSi–MoI$_2$** (**8a**). In **PMO–pycaSi** (**7**), the band assigned to the ν(C=N) stretching mode appeared at 1630 cm^{-1}; in **8a**, it was shifted to 1710 cm^{-1}. In **7**, the ν(C–H) bands were observed at 2978 and 2959 cm^{-1}.

No ν(C≡N) vibration modes corresponding to the CH_3CN ligands were found in the species obtained from reaction with **1a** or **1b**, indicating that the ligand **pycaSi** (**3**) was always coordinated in a bidentate fashion to the metal center.

The powder XRD patterns of the materials containing the MoI_2 fragment are presented in Fig. 4. The powder pattern of the parent calcined material **MCM** clearly showed four reflections in the 2θ range 2–10°, indexed to a hexagonal cell as (100), (110), (200), and (210). The d value of the (100) reflection was 35.0 Å, corresponding to a lattice constant of $a = 40.4$ Å ($= 2d_{100}/\sqrt{3}$). On functionalization of the walls of the parent host material **MCM** with ligand **3**, the powder patterns of **MCM–pycaSi** (**5**) remained almost unchanged in terms of the positions of the peaks assigned to the characteristic reflections, suggesting retention of the long-range hexagonal symmetry of the host material. The powder patterns also remained unchanged for **MCM–pycaSi–MoI$_2$** (**6a**). A reduction in the peak intensity was seen in the case of **5**, which was most relevant in the molybdenum-rich **MCM–pycaSi–MoI$_2$** (**6a**). This is attributed not to a loss of crystallinity, but rather to a reduction in the X-ray scattering contrast between the silica walls and the pore-filling material, a situation well described in the literature [42,43], and also observed for other materials [44].

The powder XRD patterns and the peak intensities for the hybrid **PMO–pycaSi** (**7**) material were similar to those of the pure siliceous matrix **MCM** parent material. Because the organic moiety was introduced during the preparation of the sol for subsequent aging, the material was obtained with a higher degree of order than when prepared by postsynthetic derivatization as **MCM–pycaSi** (**5**). This indicates that the organic moieties were well integrated within the structure of the materials.

To minimize the possible existence of richer and poorer domains of organic moieties due to segregation of phases during the aging process [16,41], methanol was added as a solvent (see the previous section). For **PMO–pycaSi–MoI$_2$** (**8a**), a slight reduction in peak intensity was seen but the structure remained unchanged, exhibiting greater ordering than **MCM–pycaSi–MoI$_2$** (**6a**) obtained with the conventional procedure.

Nitrogen adsorption studies at 77 K revealed that the pristine **MCM** sample exhibited a reversible type IV isotherm (Fig. 5) char-

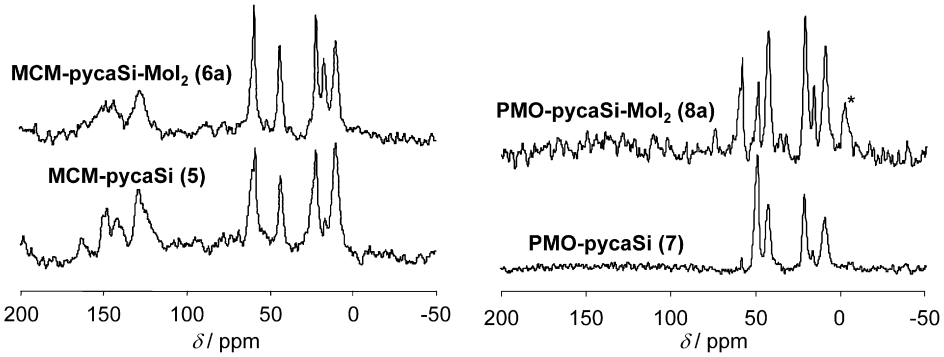

Fig. 6. Solid state ^{13}C CP MAS NMR spectra of the materials: **MCM–pycaSi** (**5**), and **MCM–pycaSi–MoI$_2$** (**6a**) (left); **PMO–pycaSi** (**7**), and **PMO–pycaSi–MoI$_2$** (**8a**) (right).

Table 2
Textural parameters for host and composite materials from N_2 isotherms at 77 K

Sample	d_{100} (Å)	S_{BET} ($m^2\ g^{-1}$)	ΔS_{BET}[a] (%)	V_P ($cm^3\ g^{-1}$)	ΔV_P[b] (%)	d_{BJH}[c] (nm)
MCM	35.0	1032	–	0.88	–	3.4
MCM–pycaSi	35.8	671	35	0.47	47	2.8
MCM–pycaSi–MoI$_2$	32.3	748	28	0.52	41	2.8
PMO–pycaSi	40.0	1069	–	1.03	–	3.8
PMO–pycaSi–MoI$_2$	37.9	925	14	0.88	15	3.8

[a] Variation of surface area in relation to parent **MCM**.
[b] Variation of total pore volume in relation to parent **MCM**.
[c] Median pore width determined by the BJH method.

acteristic of mesoporous solids (pore width 2–50 nm, according to the IUPAC) [45]. The calculated textural parameters (S_{bet} and V_P) of this material agree with literature data (Table 2) [46,47]. The capillary condensation/evaporation steps of pristine **MCM** sample occurred at a relative pressure of 0.26–0.40. The sharpness of this step reflects the uniform pore size. The isotherm of the functionalized material **MCM–pycaSi** (**5**) revealed a much lower N_2 uptake, accounting for the decreases in S_{BET} (35%) and V_P (47%).

These findings indicate that immobilization of the ligand on the internal silica surface was accomplished (Fig. 5; Table 2). For **MCM–pycaSi–MoI$_2$** (**6a**), the relative decreases in S_{BET} and V_P relative to **MCM** were 28% and 41%, respectively, in agreement with the decrease in the $p/p0$ coordinates of the inflection points of the isotherms after postsynthesis treatment [48]. The height of the capillary condensation step, which is related to the volume of pore space confined by absorbate film on the pore walls, was smaller in the modified **MCM–pycaSi** (**5**) material; furthermore, the maximum of the PSD curve (not shown) for **MCM** determined by the BJH method, d_{BJH}, decreased from 3.4 nm to <3 nm (Table 2).

The textural characteristics of the hybrid materials **PMO–pycaSi** (**7**) and **PMO–pycaSi–MoI$_2$** (**8a**) were similar to those of **MCM**, with sharp steps indicating a uniform pore size distribution.

All of the materials were characterized by solid-state NMR of ^{13}C CP MAS and ^{29}Si MAS and CP MAS. The solid-state ^{13}C CP MAS NMR spectra of **MCM–pycaSi** (**5**) and **MCM–pycaSi–MoI$_2$** (**6a**) were quite similar to those of the ligand **pyca** (**2**), confirming binding of the ligand to the surface (Fig. 6). In **MCM–pycaSi** (**5**), the peaks of the aromatic carbons were observed at 127–162 ppm, close to their positions in the free ligand, whereas all of the carbons of the linear chain were assigned to peaks at 9.5–58 ppm. The same carbon peaks were seen in the spectrum of **MCM–pycaSi–MoI$_2$** (**6a**).

The signals of the aliphatic carbons in the range ~9–60 ppm were present in the ^{13}C CP MAS NMR spectra of **PMO–pycaSi** (**7**) and **PMO–pycaSi–MoI$_2$** (**8a**), but the peaks of the aromatic carbons were not well defined, and only a broad peak could be detected. This is likely related to the small amount of **pyca** ligand in **7** (only 2.7%), as was reported for another system [16].

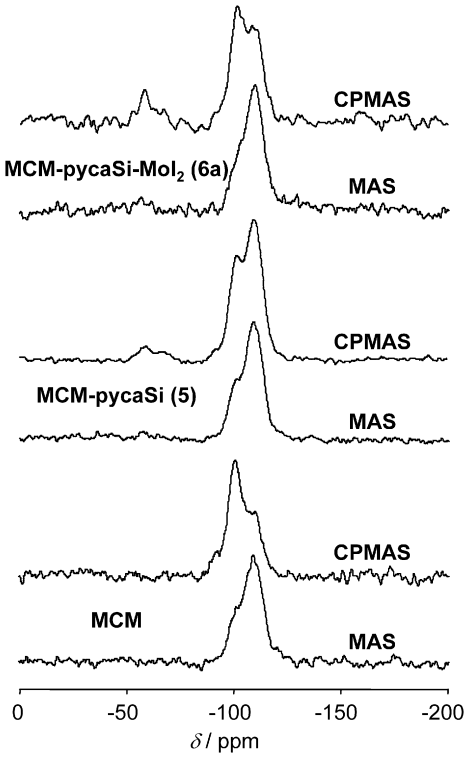

Fig. 7. ^{29}Si MAS and CP MAS NMR spectra for calcined **MCM**, **MCM–pycaSi** (**5**), and **MCM–pycaSi–MoI$_2$** (**6a**).

Fig. 7 shows the ^{29}Si MAS and CP MAS NMR spectra for pristine calcined **MCM**, **MCM–pycaSi** (**5**), and the derivatized **MCM–pycaSi–MoI$_2$** (**6a**). The unmodified **MCM** displayed two broad convoluted resonances in the ^{29}Si CP MAS NMR spectrum at −110 and −100 ppm, assigned to Q^4 and Q^3 species of the silica framework, respectively [$Q^n = Si(OSi)_n(OH)_{4-n}$]. A weak shoulder also could be seen at −91 ppm for the Q^2 species. The Q^3 sites are associated with the single silanols Si–OH (including hydrogen-bonded silanols), and the Q^2 sites correspond to the geminal silanols (Si–$(OH)_2$). The ^{29}Si CP MAS spectra of **MCM–pycaSi** (**5**) also displayed two broad signals at −58 and −60.6 ppm, assigned to T^1 and T^2 organosilica species, respectively [$T^n = RSi(OSi)_n(OEt)_{3-n}$]. A weak broad signal at −66.7 ppm can be assigned to a T^3 environment. Reaction of **MCM–pycaSi** (**5**) with the organometallic fragment [$MoI_2(CO)_3(NCCH_3)_2$] (**1a**) did not significantly change the ^{29}Si MAS and CP MAS NMR spectra, as expected.

Comparing these three materials prepared by the first approach shows that the in situ grafting of the ligand **pyca** in **MCM** to form **MCM–pycaSi** (**5**) resulted in decreased Q^2 and Q^3 resonances and a concomitant increase in Q^4 resonance compared with the par-

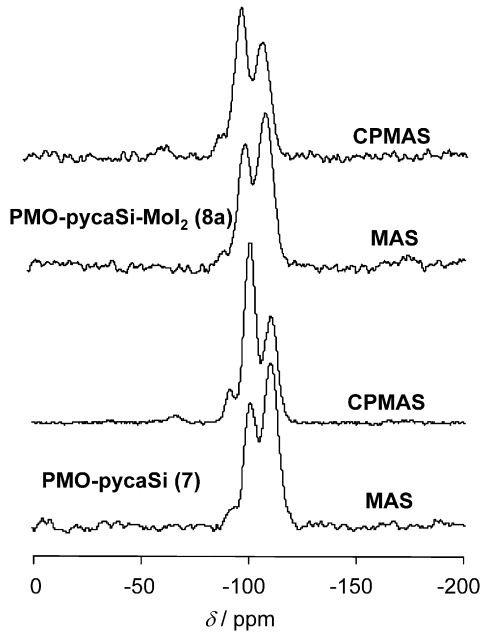

Fig. 8. ^{29}Si MAS and CP MAS NMR spectra for PMO materials **PMO–pycaSi** (**7**), and **PMO–pycaSi–MoI$_2$** (**8a**).

ent mesoporous samples (**MCM**), indicating successful ligand grafting. This trend persisted after synthesis of the derivatized material **MCM–pycaSi–MoI$_2$** (**6a**). This behavior is consistent with esterification of the isolated silanol groups (single and geminal) by nucleophilic substitution at the silicon atom in the organic ligand.

The signals shown in Fig. 8 for the PMO species are quite similar to the previous ones. The figure also shows resonances at −110.1 ppm for Q^4 and −100.6 ppm for Q^3, along with a weak shoulder at −91 ppm assigned to Q^2 species. Concerning T species, only a broad peak centered at −66 ppm can be assigned to the T^1, T^2, and T^3 species. The reaction of this material with the organometallic fragment $[MoI_2(CO)_3(NCCH_3)_2]$ (**1a**) had no significant effect on the ^{29}Si MAS and CP MAS NMR spectra compared to that of **MCM–pycaSi–MoI$_2$**, indicating that the metal fragment reacted with the immobilized ligand and did not interact with the wall surface.

3.3. Catalytic studies

The activity of both the derivatized MCM materials and the complexes $[MoX_2(CO)_3(NCCH_3)_2]$ (X = I, **1a**, X = Br, **1b**) and $[MoX_2(CO)_3(pyca)]$ (X = I, **4a**, X = Br, **4b**) as catalysts or catalyst precursors for the liquid-phase epoxidation of olefins was investigated using cyclohexene, cyclooctene, and styrene as substrates and *t*-butylhydroperoxide (TBHP) as the oxygen source, at 328 K in air, with 3 mL of dichloromethane as the solvent (Fig. 9; Table 3). The catalytic behavior remained the same when experiments were run in N_2, demonstrating that molecular dioxygen was not the oxidant, as has been reported for other systems [49].

All of the materials and complexes selectively catalyzed the oxidation of the three substrates to the corresponding epoxide with no formation of diols or ketones. These systems were even more selective than allylic Mo(II) complexes [50].

In general, the species containing Br (complexes **1b** and **4b**; materials **6b** and **8b**) were more active than the iodine analogues, a trend also observed in similar epoxidation reactions promoted by $[Mo(\eta^3\text{-allyl})(CO)_2X(N\text{–}N)]$ complexes, where the Cl derivatives proved to be more active than the bromine derivatives [50]. Moreover, the iodide derivatives were more active in epoxidation of

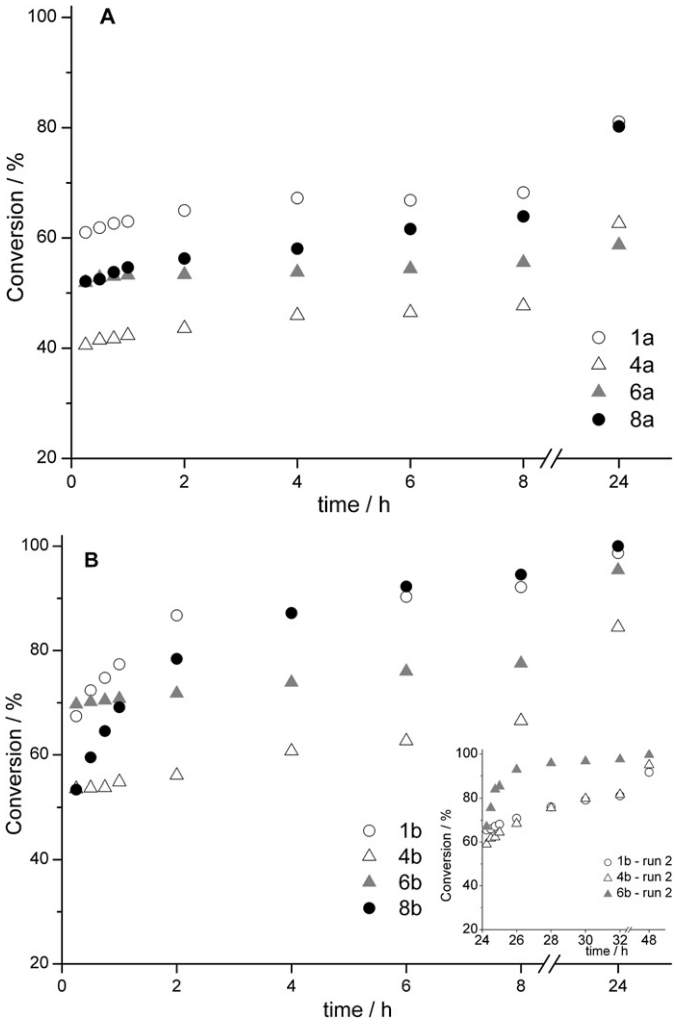

Fig. 9. Cyclooctene epoxidation using TBHP as oxygen donor, without co-solvent, at 55 °C, in the presence of $[MoX_2(CO)_3(NCCH_3)_2]$ (**1a,b**—○); $[MoX_2(CO)_3(pyca)]$ (**4a,b**—△); **MCM–pycaSi–MoX$_2$** (**6a,b**—▲); **PMO–pycaSi–MoX$_2$** (**8a,b**—●): X = I (A) and X = Br (B). Inset: the same for the second run.

styrene (Sty > Cy8 > Cy6), whereas the bromide species preferred Cy8 (Cy8 > Sty > Cy6).

The total conversions calculated after 24 h were rather high, comparable to others obtained in Mo(VI) systems, such as $MoX_2(O)_2(N\text{–}N)$, or using Mo(II) complexes as precursors [40,51,52]. The smallest conversion (61%) was found for the epoxidation of styrene catalyzed by the complex $[MoI_2(CO)_3(pyca)]$ (**4a**).

The most interesting features of the results given in Table 3 and Fig. 9 concern the high activity of the heterogeneous catalysts and the high activities exhibited in a second run when a second load of substrate and oxidant was added to the catalyst. At first glance, the homogeneous and heterogeneous catalysts seemed to exhibit similar catalytic activities, with the heterogeneous systems better than reported MCM-41-based heterogeneous systems [40,52]. Closer examination, however, reveals that some of the heterogeneous catalysts exceeded the performance of their homogeneous-phase counterparts. This is particularly evident for the epoxidation of styrene, a terminal olefin, which is known to be more difficult to oxidize than cyclic olefins by standard Mo(VI) catalysts [40]. Indeed, although the two complexes $[MoI_2(CO)_3(NCCH_3)_2]$ (**1a**) and $[MoI_2(CO)_3(pyca)]$ (**4a**) displayed conversions of 68% and 61% with TOFs of 220 and 171, respectively, in the iodine-containing materials **MCM–pycaSi–MoI$_2$** (**6a**) and **PMO–pycaSi–MoI$_2$** (**8a**) these values rose to 100% conversion of styrene with respective TOFs

Table 3
Conversions and turnover frequencies (TOF) for complexes **1a**, **1b**, **4a** and **4b** and materials **6a**, **6b**, **8a** and **8b**

Catalysts	Olefin	Conversions	TOF[a]
$[MoI_2(CO)_3(NCCH_3)_2]$ **1a**	Cy6	70	257
	Cy8	81	244
	STy	68	220
$[MoBr_2(CO)_3(NCCH_3)_2]$ **1b**	Cy6	73	274
	Cy8	100/92[b]	272/262[c]
	STy	74	226
$[MoI_2(CO)_3(pyca)]$ **4a**	Cy6	88	215
	Cy8	63	162
	STy	61	171
$[MoBr_2(CO)_3(pyca)]$ **4b**	Cy6	62	243
	Cy8	88/95[b]	215/236[c]
	STy	66	214
MCM–pycaSi–MoI_2 **6a**	Cy6	63	247
	Cy8	80	211
	STy	100	346
MCM–pycaSi–$MoBr_2$ **6b**	Cy6	73	298
	Cy8	95/100[b]	279/268[c]
	STy	77	277
PMO–pycaSi–MoI_2 **8a**	Cy6	72	265
	Cy8	82	219
	STy	100	350
PMO–pycaSi–$MoBr_2$ **8b**	Cy6	75	238
	Cy8	100	214
	STy	98	211

[a] Calcd. at 0.25 h as mol mol^{-1} [M] h^{-1}.
[b] Calcd. for the 1st run/2nd run after 24 h and 48 h.
[c] Calcd. at 0.25 h as mol mol^{-1} [M] h^{-1} for the 1st run/2nd run.

of 346 and 350. This is an outstanding result for an immobilized catalyst, and here the best catalyst bears the heavier iodine.

In the epoxidation of the cyclic olefins, the activities of homogeneous and heterogeneous catalysts did not differ significantly, although almost complete conversion was seen only in the epoxidation of cyclooctene with $[MoBr_2(CO)_3(NCCH_3)_2]$ (**1b**), rising to 100% in the corresponding material **PMO–pycaSi–MoBr$_2$** (**8b**). For cyclohexene, complex **4a** displayed the highest conversion of all catalysts (88%). All of the TOFs for the epoxidation of cyclohexene were much higher for all of the complexes **1(a,b)**, **4(a,b)** than for materials **6b** and **8b** containing the $MoBr_2$ fragment, with the iodine analogues the least active.

In addition, the **PMO**-based materials were slightly more active among the heterogeneous catalysts. These materials also have the advantage of requiring fewer preparation steps, possibly related to better-controlled quantity and distribution of the active sites, because the ligand is introduced during the synthesis of the material and not grafted afterward. The homogeneous catalysts were not selective for any of the olefins, whereas the heterogeneous catalysts exhibited higher conversions for styrene.

The second specific feature of these systems is the high conversion observed when the catalyst was reused with a new load of substrate and TBHP. This behavior was observed for the [Mo(η^3-allyl)$(CO)_2$X(N–N)] complexes when acting as precursors for the same reaction (oxidation of cyclooctene in the presence of TBHP) [50]. The results given in Table 3 indicate that the Mo(II) homogeneous catalysts achieved high conversion of cyclooctene in both the first and second runs (100/92 for the nitrile derivative and 88/95 for the **pyca** derivative), with high TOF. Even more interesting is the behavior of the supported catalyst, which led to even slightly higher conversions with higher TOFs (279/268) compared with the corresponding unsupported complex **4b** (215/236).

Our findings indicate that the active species formed were rather stable under catalysis conditions. Although the first step in the reaction is the oxidation of the Mo(II) precursor to Mo(VI) [50], and some TBHP is used for this activation, all of the complexes and materials described here are easy to handle, adding to the advantages of Mo(II) precursors for oxidation catalysis.

Table 4
Results for the polymerization reactions of NBE and Sty initiated by isolated $[Mo(CO)_3X_2(L)_2]$ and immobilized $[Mo(CO)_3X_2(L)_2]$ complexes at 333 K

Catalyst	With MAO				Without MAO			
	% Sty		% NBE		% Sty		% NBE	
	Yield	*syndio*	Yield	*cis*	Yield	*syndio*	Yield	*cis*
$[MoI_2(CO)_3(NCCH_3)_2]$ **1a**	31	29	100	41	11	29	9	39
$[MoBr_2(CO)_3(NCCH_3)_2]$ **1b**	36	29	100	63	11	22	3	67
$[MoI_2(CO)_3(pyca)]$ **4a**	36	32	22	50	8	30	2	50
$[MoBr_2(CO)_3(pyca)]$ **4b**	26	29	37	62	14	22	24	59
MCM–pycaSi–MoI_2 **6a**	40	42	86	40	10	22	3	40
MCM–pycaSi–$MoBr_2$ **6b**	29	69	29	45	3	17	3	44
PMO–pycaSi–MoI_2 **8a**	48	56	96	59	6	54	2	55
PMO–pycaSi–$MoBr_2$ **8b**	25	53	23	44	3	19	3	44

Mo(II) derivatives have received much recent attention in studies of olefin polymerization [33–37]. Complexes $[MoX_2(CO)_3(NCCH_3)_2]$ **1(a,b)** have been tested for ROMP catalysis of NBE (with polyNBE denoting the corresponding polymer product), but these and related complexes did not catalyze the ROMP reaction of NBE at 298 K [8]. Some catalytic activity was observed at 333 K (2% and 24%), with the complexes with the bromide ligand being more active than the complexes with the iodide. The same conclusions were obtained for the polymerization of styrene. Adding MAO to the catalyst enhanced the catalytic activity, as reported previously by others [53].

The results obtained for the polymerization of styrene and norbornene are given in Table 4. We should note that MAO exhibited no catalytic activity on its own (as also reported previously [8,53]). The activities in the absence of MAO were very modest. Indeed, the role of MAO is associated with transfer of a methyl group to the metal to create an active catalyst. The catalysts do not have such groups, and their formation from the monomer is not very efficient, as demonstrated by the catalytic activities. In the presence of MAO, the performance was better, especially for the ROMP of NBE, which reached 100% yield with the two nitrile complexes **1a** and **1b** and 86 and 96% with the materials containing the immobilized fragment $[MoI_2(CO)_3]$, **6a** and **8a**. Nonetheless, comparing the same complex, for instance $[MoI_2(CO)_3(pyca)]$ **4a** with its immobilized analogues **MCM–pycaSi–MoI$_2$ 6a** and **PMO–pycaSi–MoI$_2$ 8a**, shows that the yield increased from 22% to 86% and 96%. None of the systems displayed high selectivity, with the percentages of *cis*-polyNBE and *syndio*-polystyrene being close to statistic.

Overall, the heterogeneous catalysts performed better than the homogeneous catalysts, contributing to the advantages of such systems, including ease of recycling and separation and, in this case, higher product yields.

4. Conclusion

Complexes $[MoX_2(CO)_3(pyca)]$ (X = I, **4a**, X = Br, **4b**) with pyca = $C_5H_4NCH{=}N(CH_2)_2CH_3$ (**2**) were prepared and immobilized in MCM-41. In the immobilization procedure, the silylated ligand $C_5H_4NCH{=}N(CH_2)_3Si(OEt)_3$ (pycaSi, **3**) was used. In the first approach, it was grafted on the wall of **MCM** (**MCM–pycaSi**) and allowed to react with the metal precursors **1a** and **1b** to afford the new materials **MCM–pycaSi–MoX$_2$** (X = I, **6a**, X = Br, **6b**). In the second approach, a PMO-type material was prepared in one pot, containing the ligand in the material (**PMO–pycaSi**), followed by reaction with complexes **1a** and **1b**, to yield **PMO–pycaSi–MoX$_2$** (X = I, **8a**, X = Br, **8b**). All of the materials displayed the features of ordered mesoporous materials observed in the parent **MCM**, as

shown by XRD and N_2 adsorption isotherms, and ca. 2.7–5.4% of molybdenum was loaded in **6a,b** and **8a,b**.

The catalytic activity of the complexes and the metal-containing materials was tested in olefin oxidation in the presence of *t*-butylhydroperoxide and styrene polymerization and ROMP of NBE. The polymerization reactions required the presence of MAO, and the yields were high for ROMP of NBE catalyzed in homogeneous phase by the nitrile complexes $[MoX_2(CO)_3(NCCH_3)_2]$ (X = I, **1a**, X = Br, **1b**) and the iodine-containing materials **6a** and **8a**, although the selectivity was low.

The oxidation catalysis produced very interesting results. In general, all of the homogeneous and heterogeneous catalysts achieved high conversions, with the highest ones in the latter. The iodine-containing species were particularly active toward styrene oxidation, with a much better performance associated with the supported catalysts. Other important features of the system include high activity in a second run of the catalyst and high selectivity toward epoxide formation (100%).

Our findings demonstrate that the new materials described in this work are excellent precursors for the oxidation catalysis of olefins using an TBHP as oxidant. Although some may object that Mo(II) complexes are not appropriated for this chemistry, these can be easily converted in Mo(VI) species, which are stable under catalytic conditions (maintaining high activity in the second run) and are easily handled. This same behavior was observed in another family of Mo(II) precursors, suggesting a similar mechanism based on dioxo complexes [50]. These react with TBHP, on the addition of the OH bond to Mo=O, to form a complex with OOR and OH ligands [54], which then interacts with the olefin to yield epoxide selectively. In addition, the immobilization of these complexes by anchoring the silylated ligand in MCM leads to even more active catalyst materials, which combine the activity and selectivity of the homogeneous system with the general advantages of heterogeneous catalysts.

Supplementary material

Crystallographic data for the structural analysis of $[Zn(pyca)Cl_2]$ has been deposited at the Cambridge Crystallographic Data Center, 12 Union Road, Cambridge, CB21EZ, UK, and are available free of charge on request quoting the deposition number CCDC 668186 (Fax: +44 1223 336033, e-mail address: deposit@ccdc.cam.ac.uk).

Acknowledgments

This work was supported by FCT research grants SFRH/BPD/-27344/2006 (to C.D.N.) and SFRH/BPD/28149/2006 (to P.D.V.). The authors thank J. Pires and A.P. Carvalho of CQB for their kind help with the adsorption measurements.

References

[1] C.T. Kresge, M.E. Leonowicz, W.J. Roth, J.C. Vartuli, J.S. Beck, Nature 359 (1992) 710.
[2] J.S. Beck, J.C. Vartuli, W.J. Roth, M.E. Leonowicz, C.T. Kresge, K.D. Schmitt, C.T.W. Chu, D.H. Olson, E.W. Sheppard, S.B. McCullen, J.B. Higgins, J.L. Schlenker, J. Am. Chem. Soc. 114 (1992) 10834.
[3] M.H. Valkenberg, W.F. Hölderich, Catal. Rev. 44 (2002) 321.
[4] D.M. Ford, E.E. Simanek, D.F. Shantz, Nanotechnology 16 (2005) S458.
[5] C.D. Nunes, M. Pillinger, A.A. Valente, I.S. Gonçalves, J. Rocha, P. Ferreira, F.E. Kühn, Eur. J. Inorg. Chem. (2002) 1100.
[6] M. Pillinger, C.D. Nunes, P.D. Vaz, A.A. Valente, I.S. Gonçalves, P.J.A. Ribeiro-Claro, J. Rocha, L.D. Carlos, F.E. Kühn, Phys. Chem. Chem. Phys. 4 (2002) 3098.
[7] T.A. Fernandes, C.D. Nunes, P.D. Vaz, M.J. Calhorda, P. Brandão, J. Rocha, I.S. Gonçalves, A.A. Valente, L.P. Ferreira, M. Godinho, P. Ferreira, Micropor. Mesopor. Mater. (2007), doi:10.1016/j.micromeso.2007.09.009.
[8] J. Gimenez, C.D. Nunes, P.D. Vaz, A.A. Valente, P. Ferreira, M.J. Calhorda, J Mol. Catal. A 256 (2006) 90.
[9] S.R. Hall, C.E. Fowler, B. Lebeau, S. Mann, Chem. Commun. (1999) 201.
[10] B. Hatton, K. Landskron, W. Whitnall, D. Perovic, G.A. Ozin, Acc. Chem. Res. 38 (2005) 305.
[11] W.J. Hunks, G.A. Ozin, J. Mater. Chem. 15 (2005) 3716.
[12] H.-W. Jeong, C.-H. Kwak, I.-Kim, C.-S. Ha, S.-D. Seul, Mol. Cryst. Liq. Cryst. 425 (2004) 173.
[13] E. Besson, A. Mehdi, D.A. Lerner, C. Reyé, R.J.P. Corriu, J. Mater. Chem. 15 (2005) 803.
[14] O. Olkhovyk, M. Jaroniec, J. Am. Chem. Soc. 127 (2005) 60.
[15] O. Olkhovyk, S. Pikus, M. Jaroniec, J. Mater. Chem. 15 (2005) 1517.
[16] C.D. Nunes, P.D. Vaz, P. Brandão, J. Rocha, P. Ferreira, N. Bion, M.J. Calhorda, Micropor. Mesopor. Mater. 95 (2006) 104.
[17] P. Ferreira, C.D. Nunes, P.D. Vaz, N. Bion, P. Brandão, J. Rocha, Prog. Solid State Chem. 33 (2005) 162.
[18] C. Yoshina-Ishii, T. Asefa, N. Coombs, M.J. MacLachlan, G.A. Ozin, Chem. Commun. (1999) 2539.
[19] N. Bion, P. Ferreira, A.A. Valente, I.S. Gonçalves, J. Rocha, J. Mater. Chem. 13 (2003) 1910.
[20] G. Temtsin, T. Asefa, S. Bittner, G.A. Ozin, J. Mater. Chem. 11 (2001) 3202.
[21] Y. Goto, S. Inagaki, Chem. Commun. (2002) 2410.
[22] M.P. Kapoor, Q. Yang, S. Inagaki, Chem. Mater. 16 (2004) 1209.
[23] M. Kuroki, T. Asefa, W. Whitnal, M. Kruk, C. Yoshina-Ishii, M. Jaroniec, G.A. Ozin, J. Am. Chem. Soc. 124 (2002) 13886.
[24] M.P. Kapoor, N. Setoyama, Q. Yang, M. Ohashi, S. Inagaki, Langmuir 21 (2005) 443.
[25] M. Jia, A. Seifert, M. Berger, H. Giegengack, S. Schulze, W.R. Thiel, Chem. Mater. 16 (2004) 877.
[26] K. Landskron, G.A. Ozin, Science 306 (2004) 1529.
[27] C. Sanchez, G.J. de A.A. Soler-Illia, F. Ribot, T. Lalot, C.R. Mayer, V. Cabuil, Chem. Mater. 13 (2001) 3061.
[28] P.D. Vaz, C.D. Nunes, M. Vasconcellos-Dias, M.M. Nolasco, P.J.A. Ribeiro Claro, M.J. Calhorda, Chem. Eur. J. 13 (2007) 7874.
[29] P.K. Baker, M.B. Hursthouse, A.I. Karaulov, A.J. Lavery, K.M.A. Malik, D.J. Muldoon, A. Shawcross, J. Chem. Soc. Dalton Trans. (1994) 3493.
[30] C.D. Nunes, A.A. Valente, M. Pillinger, A.C. Fernandes, C.C. Romão, J. Rocha, I.S. Gonçalves, J. Mater. Chem. 12 (2002) 1735.
[31] M. Kruk, M. Jaroniec, Langmuir 13 (1997) 6267.
[32] M. Kruk, V. Antochshuk, M. Jaroniec, J. Phys. Chem. B 103 (1999) 10670.
[33] M. Al-Jahdali, P.K. Baker, A.J. Lavery, M. Meehan, D.J. Muldoon, J. Mol. Catal. A: Chem. 159 (2000) 51.
[34] P.K. Baker, M.A. Beckett, B.M. Stiefvater-Thomas, J. Mol. Catal. A: Chem. 193 (2003) 77.
[35] T. Szymánska-Buzar, T. Glowiak, I. Czelúsniak, J. Organomet. Chem. 640 (2001) 72.
[36] T. Szymánska-Buzar, T. Glowiak, I. Czelúsniak, Polyhedron 21 (2002) 2505.
[37] I. Czelúsniak, T. Szymánska-Buzar, Appl. Catal. A 277 (2004) 173.
[38] G.M. Sheldrick, SHELX-97, University of Göttingen, 1997.
[39] A.L. Spek, PLATON program, J. Appl. Cryst. 36 (2003) 7.
[40] C.D. Nunes, M. Pillinger, A.A. Valente, J. Rocha, A.D. Lopes, I.S. Gonçalves, Eur. J. Inorg. Chem. (2003) 3870.
[41] M.T. Anderson, J.E. Martin, J.G. Odinek, P.P. Newcomer, Chem. Mater. 10 (1998) 1490.
[42] B. Marler, U. Oberhagemann, S. Voltmann, H. Gies, Micropor. Mater. 6 (1996) 375.
[43] W. Hammond, E. Prouzet, S.D. Mahanti, T.J. Pinnavaia, Micropor. Mesopor. Mater. 27 (1999) 19.
[44] M. Vasconcellos-Dias, C.D. Nunes, P.D. Vaz, P. Ferreira, M.J. Calhorda, Eur. J. Inorg. Chem. (2007) 2917.
[45] S.J. Gregg, K.S.W. Sing, in: Adsorption, Surface Area and Porosity, second ed., Academic Press, London, 1982.
[46] M.D. Alba, A. Becerro, J. Klinowski, J. Chem. Soc., Faraday Trans. 92 (1996) 849.
[47] A.A. Romero, M.D. Alba, W. Zhou, J. Klinowski, J. Phys. Chem. B 101 (1997) 5294.
[48] M. Kruk, M. Jaroniec, Langmuir 15 (1999) 5410.
[49] M.D. Hughes, Y.-J. Xu, P. Jenkins, P. McMorn, P. Landon, D.I. Enache, A.F. Carlay, G.A. Attard, G.J. Hutchings, F. King, E.H. Stitt, P. Jonhnston, K. Griffin, C.J. Kiely, Nature 437 (2005) 1132.
[50] J.C. Alonso, P. Neves, M.J. Pires da Silva, S. Quintal, P.D. Vaz, C. Silva, A.A. Valente, P. Ferreira, M.J. Calhorda, V. Félix, M.G.B. Drew, Organometallics 26 (2007) 5548.
[51] J. Zhao, A.M. Santos, E. Herdtwerk, F.E. Kühn, J. Mol. Catal. A: Chem. 222 (2004) 265.
[52] C.D. Nunes, A.A. Valente, M. Pillinger, J. Rocha, I.S. Gonçalves, Chem. Eur. J. 9 (2003) 4380.
[53] H. Rahiala, I. Beurroies, T. Eklund, K. Hakala, R. Gougeon, P. Trens, J.B. Rosenholm, J. Catal. 188 (1999) 14.
[54] L.F. Veiros, Â. Prazeres, P.J. Costa, C.C. Romão, F.E. Kühn, M.J. Calhorda, Dalton Trans. (2006) 1383.